

This article was downloaded by: [Canadian Research Knowledge Network]

On: 9 September 2010

Access details: Access Details: [subscription number 918588849]

Publisher Taylor & Francis

Informa Ltd Registered in England and Wales Registered Number: 1072954 Registered office: Mortimer House, 37-41 Mortimer Street, London W1T 3JH, UK



Polymer Reviews

Publication details, including instructions for authors and subscription information:

<http://www.informaworld.com/smpp/title~content=t713597276>

Advances in the Transmission Electron Microscopy of Polymers

Matthew R. Libera^a; Ray F. Egerton^b

^a Department of Chemical Engineering and Materials Science, Stevens Institute of Technology, Hoboken, New Jersey ^b Department of Physics, University of Alberta, Edmonton, Canada

Online publication date: 17 August 2010

To cite this Article Libera, Matthew R. and Egerton, Ray F.(2010) 'Advances in the Transmission Electron Microscopy of Polymers', Polymer Reviews, 50: 3, 321 – 339

To link to this Article: DOI: 10.1080/15583724.2010.493256

URL: <http://dx.doi.org/10.1080/15583724.2010.493256>

PLEASE SCROLL DOWN FOR ARTICLE

Full terms and conditions of use: <http://www.informaworld.com/terms-and-conditions-of-access.pdf>

This article may be used for research, teaching and private study purposes. Any substantial or systematic reproduction, re-distribution, re-selling, loan or sub-licensing, systematic supply or distribution in any form to anyone is expressly forbidden.

The publisher does not give any warranty express or implied or make any representation that the contents will be complete or accurate or up to date. The accuracy of any instructions, formulae and drug doses should be independently verified with primary sources. The publisher shall not be liable for any loss, actions, claims, proceedings, demand or costs or damages whatsoever or howsoever caused arising directly or indirectly in connection with or arising out of the use of this material.

Advances in the Transmission Electron Microscopy of Polymers

MATTHEW R. LIBERA¹ AND RAY F. EGERTON²

¹Department of Chemical Engineering and Materials Science, Stevens Institute of Technology, Hoboken, New Jersey

²Department of Physics, University of Alberta, Edmonton, Canada

Transmission electron microscopy (TEM) of polymers involves the problem definition and methodologies associated with the microscopy of both inorganic and biological materials but cannot be categorized within either of these fields alone. On the one hand, like other synthetic materials, polymers offer the ability to control properties through synthesis and processing, and TEM is a powerful method with which to provide information within the synthesis–structure–property paradigm of materials science and engineering. The well-established techniques of bright/dark-field imaging, electron diffraction, high-resolution imaging, and analytical microscopies are thus all used to study polymers. On the other hand, the electron–specimen interactions are more like those in biological systems. Synthetic polymers and biological materials consist largely of light elements whose elastic interactions with energetic electrons are relatively weak. Generating image contrast can thus be a challenge in polymer TEM. The inelastic electron/soft material interactions are, however, relatively strong. These provide for powerful spectroscopies but also lead to radiation damage. The constraints that damage puts on imaging are far more stringent in polymers than in inorganic systems. This review highlights ongoing advances in contrast generation exploiting both elastic and inelastic electron–polymer interactions and outlines the salient issues determining the achievable spatial resolution in radiation-sensitive materials.

Keywords polymer, TEM, electron microscopy, radiation damage, image contrast, image resolution, holography, phase contrast, stain

1. Introduction

The transmission electron microscope (TEM) has been used extensively for decades to study the morphology of synthetic polymers. It continues to be an essential tool, particularly because of the inherent ability of these materials to hierarchically structure themselves over multiple length scales and produce morphologies that lead to advances in functionality and application. Significantly, instrumentation advances over the past decade have made both established and emerging TEM imaging methods more accessible to an ever-growing number of applications-oriented research groups around the world, and increasing numbers of scientists and engineers are exploiting these methods to quantify polymer morphology.

Received February 10, 2010; accepted April 15, 2010.

Address correspondence to Matthew Libera, Department of Chemical Engineering and Materials Science, Stevens Institute of Technology, 1 Castle Point Terrace, Hoboken, NJ 07030. E-mail: mlibera@stevens.edu

There have historically been two central challenges associated with studying polymers in the electron microscope. First, because they are predominantly comprised of low-atomic-number elements, soft materials display an intrinsically low level of electron-optical image contrast. Second, soft materials tend to be very sensitive to the ionizing radiation used in an intermediate-energy electron microscope and can suffer both chemical and structural change—beam damage—during the microstructural measurement. These two issues continue to provide an incentive to the development of new imaging techniques.

A number of excellent and modern monographs have been written on transmission electron microscopy and its application to materials^{1–3} and two important ones that focus primarily on polymers.^{4,5} This review highlights some of the most advanced work over the past decade, concentrating on new methods to generate contrast, advances in our understanding of radiation damage in the TEM, and the increasingly important topic of dose-limited spatial resolution.

2. Contrast Mechanisms

Some of the basic contrast mechanisms afforded by electron–specimen interactions are outlined schematically by Figure 1. A subset of soft materials exhibits spatial variations in crystallinity, crystal orientation, or density due to the presence of heavy elements. Crystallinity gives rise to Bragg diffraction, and heavy elements can induce significant Rutherford scattering. In both cases, some incident electrons are scattered to relatively high angles where they can be blocked by an objective aperture (Figure 1A), thus producing dark contrast in a final image. In many cases, however, soft-material specimens are amorphous and do not exhibit significant spatial variations in density. Thus, scattering is primarily in the forward direction, and an objective aperture provides little or no contrast. Nevertheless, the rich valence electron structure of soft materials can introduce spatial modulations in the phase or energy of an incident electron wave (Figure 1B). These provide two alternate sources of contrast for imaging soft-materials morphology, and much of the recent and ongoing technique-development work concentrates on phase contrast and spectroscopic

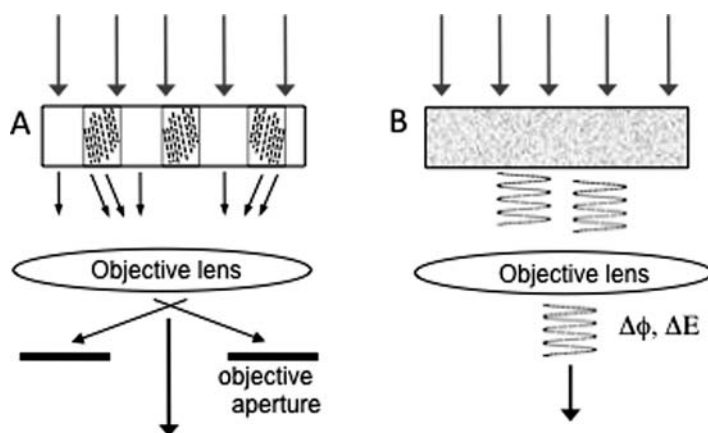


Figure 1. (A) Spatially modulated crystallinity or heavy element stain distribution provides for amplitude contrast when electrons scattered to high angles are blocked by the objective aperture. (B) Changes in electron phase or in electron energy are alternative sources of contrast in amorphous soft materials with small variations in density.

imaging methods. The following few sections outline and review some of the important aspects of these various imaging methods.

2.1. Bragg Diffraction

Diffraction-contrast imaging techniques well established in crystalline inorganic systems have been used extensively to study crystalline and semicrystalline polymers. These have recently been discussed by Michler.⁴ High-resolution imaging methods, based on the interference of two or more Bragg-scattered beams, have been described by Martin et al.^{6,7}

2.2. Heavy Element Stains

Heavy element staining coupled with bright-field imaging has been used for decades to study polymer morphology.^{5,8} This method takes advantage of the fact that certain elements or compounds will preferentially react with or localize themselves in some particular component of a polymeric material. Osmium tetroxide, for example, reacts with unsaturated carbon-carbon bonds, whereas ruthenium tetroxide preferentially reacts with aromatic rings. Figure 2 illustrates the significant contrast induced by OsO₄ staining of a microphase-separated nanoparticle blend of homopolymer polystyrene (PS) and polystyrene-polybutadiene-polystyrene (SBS) triblock copolymer. Other common stains include iodine, uranyl acetate, and phosphotungstic acid. All of them to varying degrees tend to preferentially localize within specimen regions of lower density such as the amorphous parts of semicrystalline polymers.⁹ The nature and use of these and other stains have been reviewed by Sawyer et al.⁵ and by Smith and Bryg.⁸

All of these stains induce contrast by preferentially scattering electrons elastically to high angles. For a uranium atom, the median angle for elastic scattering of 100 keV electrons is about 50 mrad, so a small objective aperture will intercept almost all of these electrons, making uranium-stained regions much more opaque than any surrounding unstained specimen regions.

Because of the various complex morphologies that can be displayed over a range of length scales by and, indeed, engineered into, polymeric materials, three-dimensional imaging using transmission electron tomography has been of growing importance. Tomographic imaging is particularly useful in studies of block copolymers where microphase separation occurs at nanolength scales to produce interpenetrated three-dimensional morphologies difficult to analyze by traditional two-dimensional techniques. Much of this work can take great advantage of stained specimens, which produce high contrast and are relatively insensitive to electron-beam damage. Tomography produces a three-dimensional image by reconstructing a large number of two-dimensional images collected from the same specimen but from a large range of different angles.¹⁰ Some of the first applications to synthetic polymers were made by Spontak et al.^{11,12} in the mid 1990s. The integration of powerful computer systems and fully motorized specimen stages on the current generation of microscopes has made the technique far more accessible and its use in polymer-morphology studies continues to accelerate.¹³

Despite the fact that staining methods have been and will no doubt continue to be used by polymer microscopists, there are several shortcomings associated with their use. Among these is the fact that they are inherently qualitative. Often, a qualitative understanding of morphology is adequate, but sometimes it is not. In addition, stains can introduce artifacts such as inorganic nanostructures¹⁴ or nonlinear decoration of interfaces,¹⁵ and care must often be exercised when interpreting stain-induced contrast. Perhaps most importantly,

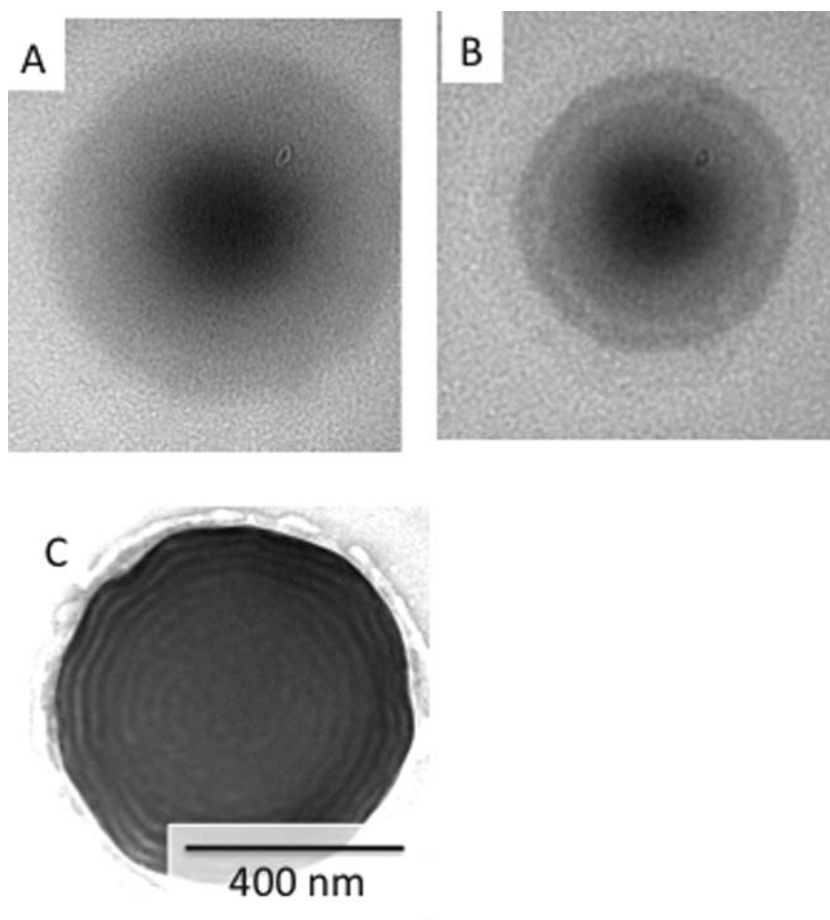


Figure 2. Bright-field TEM (200 keV) images of the same SBS triblock copolymer–PS homopolymer nanoparticle blend on a carbon support film: (A) unstained, near focus; (B) unstained at $-35\ \mu\text{m}$ defocus; (C) OsO_4 stained at focus.

however, is the simple fact that there are no good stains for many polymer systems. The various components in some systems often have similar structures and chemistries, limiting the extent to which a particular stain can preferentially label one or more of these components in an interpretable manner. Furthermore, there is increasing interest in studying materials under conditions related to their synthesis or use, such as solvation or hydration, and most staining protocols have limited utility under such conditions. Consequently, there is interest in exploring alternative imaging methods that forego the use of stains and instead generate contrast based on the intrinsic interaction of incident electrons with the polymer specimen itself.

2.3. Phase Contrast

In the absence of stains, one alternative source of contrast lies in differential modulations of the electron phase. Phase modulation occurs because the positive Coulombic potential of an atomic nucleus accelerates the incident electron wave. The Coulombic potential can be

represented as a Fourier series, and the orientation-independent zeroth-order term in this series is referred to as the mean inner potential, Φ_0 . An electron-optical index of refraction, n_{eo} , can be defined as:

$$n_{eo} = 1 + \frac{e\Phi_0}{E} \frac{E_0 + E}{2E_0 + E} \quad (1)$$

where e is the magnitude of the electron charge, E is the accelerating energy, and E_0 is the electron rest energy. Relative to a reference wave that would pass through vacuum rather than through a specimen, and in the absence of dynamical-scattering effects, the electron phase is shifted by an amount:

$$\Delta\phi = 2\pi (n_{eo} - 1) (t/\lambda) \quad (2)$$

where t is the specimen thickness and λ is the electron wavelength. Specimen-dependent spatial variations in Φ_0 will thus give rise to spatial variations in $\Delta\phi$ and thus to phase contrast.

A lot of work has been done related to models and measurements of the mean inner potential for various materials, much of which has concentrated on inorganic solids. Gadjariska-Josifovska and Carim have provided an excellent overview of much of this work.¹⁶ Φ_0 varies from approximately 5 to 30 V. It has been measured to be 8.5 V in polystyrene,¹⁷ 9.09 V in amorphous carbon,¹⁸ and 5.9 V and 5.4 V in anthracene and naphthalene,¹⁹ respectively. Though the magnitude of the mean inner potential is in great measure determined by the nuclear charge, subtle variations in Φ_0 are related to the redistribution of valence electrons and this effect is the source of phase contrast in many organic polymers and other soft materials. In the absence of thickness differences or significant variations in density, organic materials provide a range of possible valence states. At one extreme is carbon in the fully saturated state, such as found in polyethylene; the other extreme is carbon in a highly conjugated state with delocalized electron states, such as found in polythiophene or polyanilene.

Because the information recorded on film or on a charge-couple device (CCD) camera corresponds to the modulus squared of the exit-face wave function, modified by the imaging lenses of the microscope, phase information is lost. The three main techniques used to convert phase information into amplitude information are defocusing, holographic methods, and methods that use some form of Zernike phase plate. All three approaches have been explored in the context of imaging the morphology of amorphous multiphase polymers.

Defocusing is a classic technique that employs defocus on the order of 10 μm or more to force the objective-lens transfer properties to convert phase information into amplitude information. It is a method well established in biological systems. It was applied to polymers in the mid 1970s by Petermann and Gleiter²⁰ and used extensively by Petermann until 2002.²¹ In the early 1980s Thomas et al. applied defocus phase-contrast imaging to a variety of different polymers including polystyrene-polyisoprene (PS-PI) block copolymer systems.^{22–25} The technique has recently been discussed by Simon et al.²⁶ Figure 2B shows that a defocus of about 35 μm is able to generate phase contrast in the SBS-PS nanoparticle blend. The nature of this contrast, however, bears little direct correspondence to the nanoscale morphology manifested by OsO₄ staining (Figure 2C). Defocus imaging has not been extensively used in polymer studies for two reasons. First, the achievable resolution degrades as the defocus increases. Second, the transfer properties of the objective lens become very nonlinear at high defocus and can thus introduce contrast inversions that complicate image interpretation.

A second method to study polymers and soft materials by phase-contrast imaging is off-axis transmission electron holography.^{27,28} In contrast to the defocus method, holography can be done with the specimen either in focus or very close to focus. It was first conceived of by Dennis Gabor in 1947 to improve the resolution of a TEM. Based on the interference between an object wave that passes through a specimen and a reference wave that passes through the vacuum adjacent to the specimen, holography is a technique particularly well suited to phase-contrast imaging. The advent of coherent light sources—lasers—in the early 1960s enabled great progress in light-based holography. Electron holography did not make much impact until the late 1980s when coherent electron sources—field-emission gun (FEG) sources—became commercially available and thus accessible to many researchers. It has found some good success imaging magnetic and electrostatic fields. First applied to polymers in the mid-1990s,^{29–31} holography has been used to study a variety of polymeric systems over the past decade.^{26,32–36} Significantly, the Lichte group has shown that holographic phase-contrast imaging can differentiate phase shifts generated by the subtle differences in mean inner potential between polystyrene and polyisoprene in an SIS block copolymer.²⁶

Though holography can provide for both high-resolution and quantitative imaging, it has seen relatively little application to polymers. This is in part due to the need for somewhat specialized instrumentation, including a field-emission microscope and an electron biprism. In addition, to obtain an unmodulated reference wave that travels through a vacuum means that only regions of specimen within a few micrometers of an edge can be studied. Even more limiting, however, is the fact that the field of view is limited to hundreds of nanometers when using the standard objective lens and to $\sim 1\text{--}2\ \mu\text{m}$ when using a so-called post-specimen Lorentz lens. Consequently, though holographic imaging may prove particularly useful for imaging polymeric nanostructures, it currently is less useful for studying the mesoscale structure that is so important in a great majority of polymer applications.

A third method for phase-contrast imaging involves the use of a post-specimen phase plate inserted at the back-focal plane of the objective lens. The phase plate can take the form of a uniform film of conducting material (e.g., carbon) of suitable thickness, usually chosen to change the phase of scattered electrons by $\pi/2$, with a small axial hole such that the phase of the forward-scattered beam is unaltered.³⁷ Alternatively, it can be a three-electrode structure acting as a miniature einzel lens.^{38,39} In both cases, problems have arisen from hydrocarbon contamination and/or charging of the phase plate, leading to unstable properties. In addition, the central hole is often not small enough, so that information of low spatial frequency is lost. However, research on phase plates continues because of the potential to provide adequate image contrast at lower dose.⁴⁰ As with holography, the specimen can be sharply focused, and resolution is therefore optimized. Figure 3, for example, shows a phase-contrast image, taken at focus, of an unstained lamellar PS-PI diblock copolymer.⁴¹ Note that this image shows adequate contrast to resolve the two phases, but by itself it does not enable one to determine which phase corresponds to the PS and which to the PI.

2.4. Spectroscopic Contrast

The inelastic interactions between energetic electrons and materials provide an alternative source of contrast for quantitative mapping of composition, chemistry, and the distribution of phases in materials without the need for heavy-element stains. These interactions can be analyzed by electron energy-loss spectroscopy (EELS).^{42–44} Significantly, the past two decades have seen substantial improvements in both the hardware used to collect EELS

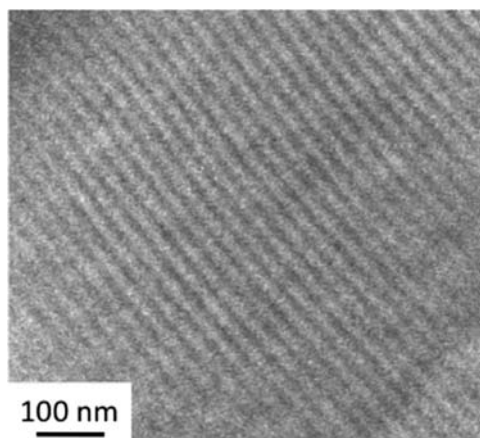


Figure 3. Phase contrast image of an unstained lamellar polystyrene–polyisoprene diblock copolymer (PS-*b*-PI) collected using a 300-kV microscope equipped with a semicircular phase plate (after Tosaka et al.⁴¹).

data and the software used to analyze it, so spectroscopic imaging has become far more accessible to applications-oriented engineers and scientists.

Electron energy-loss spectroscopy in the TEM is particularly well suited for analyzing energy losses in the sub-keV regime. This range includes K-shell core excitations from carbon (284 eV), oxygen (532 eV), and nitrogen (401 eV), as well as L-shell and M-shell excitations from a wide range of higher atomic number elements.⁴⁴ Most soft materials have high concentrations of carbon, nitrogen, oxygen, and hydrogen, and the electronic structure associated with macromolecular compounds of these elements leads to distinctive fine structure in the ionization edges. Often, different polymer phases can be distinguished from each other based on their relative compositions. Significantly, the multiple hybrid bonding states characteristic of carbon, in particular, provide a rich valence-electron fine structure in soft materials. Low-loss spectra—sampling energy losses between a few eV and about 50 eV where valence states manifest themselves—provide a second type of characteristic fingerprint that can be used to differentiate between different polymer phases based on their relative chemistries.

The magnitudes of inelastic electron scattering cross sections scale inversely with the energy loss ΔE . Consequently, the spectroscopic intensity associated with low-loss spectra is orders of magnitude higher than that associated with core-loss spectra. Under conditions of dose-limited resolution typical of radiation-sensitive soft materials, as discussed below, a substantially higher signal and better spatial resolution can often be achieved using low-loss rather than core-loss spectroscopy.

Imaging based on spectroscopic contrast can be performed in either scanning transmission electron microscope (STEM) mode using spectrum imaging^{45,46} or in TEM mode using energy-filtering (EFTEM) techniques.^{47,48} EELS spectrum imaging collects a continuous energy-loss spectrum over a range of energies (e.g., 0 to 80 eV loss) at each pixel in a 2D digital raster over a specimen area. Having complete spectra brings advantages to background modeling and fitting. In addition, all of the inelastically scattered electrons in the collection range can contribute to the imaging, so the incident dose is used most efficiently. In contrast, energy filtering uses either an in-column or post-column filter to collect images using electrons from a defined energy window, often 5–10 eV wide. EFTEM

has repeatedly proven powerful for so-called zero-loss imaging, where most inelastically scattered electrons are filtered out using a slit centered on the zero-loss peak. It is similarly useful for core-loss imaging to map elemental distribution but is less useful for mapping chemical variations, because these require an energy resolution of a few eV or less. Because a large fraction of inelastic electrons is filtered from the final image, the incident dose is used less efficiently than in spectrum imaging mode.

Energy-loss spectroscopy and its application to polymers has been reviewed by Du Chesne⁴⁹ and by Libera and Disko,⁵⁰ and over the past decade there has been steady interest in the use of this technique. It has, for example, been used extensively, both in core-loss and low-loss modes, to study several aspects of multiphase polymer morphology in various types of blends, composites and block copolymers.^{51–60} In addition, spatially resolved EELS has been applied to studies of a variety of polymer–polymer and polymer–inorganic interfaces.^{61–68} By incorporating cryo-TEM techniques that have been well established in the biological microscopy community and by exploiting the fact that solvents can have characteristic spectral fingerprints substantially different than those of many polymers,^{69,70} spatially resolved EELS has also been applied to a number of frozen-hydrated^{71–74} and frozen-solvated materials.^{75,76} Figure 4 provides an example of the problem-solving power of this approach. It summarizes results related to the colloidal synthesis of biphasic poly(dimethyl siloxane) [PDMS]-acrylate copolymer nanoparticles.^{71,74} Figure 4A shows that the water, PDMS, and acrylate low-loss EELS spectra can be distinguished from each other. Water, for example, displays a sharp onset circa 9 eV loss, which has been attributed to excitation across the band gap^{69,77} and which effectively differentiates water spectroscopically from many soft materials. Component mapping by cryo-spectrum imaging (Figures 4B–D) shows that acrylate monomer dissolves in the PDMS host precursor. The formation of lobed-type emulsions via the copolymerization of acrylate monomers in a PDMS seed emulsion was confirmed using a high-angle annular-dark-field (HAADF) STEM image (Figure 4E), and subsequent component mapping (Figure 4F) shows the formation of the biphasic nanoparticle with PDMS-rich and polyacrylate-rich lobes. Significantly, however, the copolymer-rich lobe in this biphasic colloid consists of almost pure organic copolymer, whereas the PDMS-rich lobe is partly mixed with the copolymer. This result indicates that the interphase boundary is highly diffuse, a finding that provides important insight into the synthesis–structure–property relationships in this particular polymer system.

One instrumentation development that will no doubt have a significant impact on the contrast associated with spectroscopic imaging of polymers is the commercial availability of monochromators.^{78–84} Typically, the energy resolution associated with EELS-based methods is limited by the energy spread of the electron source, represented by the full-width at half-maximum of the zero-loss peak in an energy-loss spectrum. The energy spread of a Schottky thermally assisted field-emission gun (FEG) electron source is typically about 0.6–1.0 eV. Cold field emission sources have a narrower spread (~0.3–0.4 eV) due to their lower temperature, whereas thermionic sources (W or LaB₆) have energy spreads of about 1.5 eV or more. Monochromators filter the emitted electrons at the price of a reduced incident current, and energy resolutions on the order of 0.1 eV can be achieved, sufficient to resolve substantially more fine structure in energy-loss spectra. Figure 5 presents spectra collected from polystyrene using monochromated and unfiltered electrons. The enhanced energy resolution enables the low-energy shoulder (~5.5 eV) on the $\pi-\pi^*$ peak (~7 eV) as well as a series of interband transitions on the rising edge of the bulk plasmon peak to be detected. Early work using monochromated electron sources was performed by the Boersch group, with sub-10-meV energy resolution,^{79,85} The Ritsko et al.^{86,87} and Fink et al.^{88,89} studies were not done using an electron microscope and, hence, lacked spatial resolution.

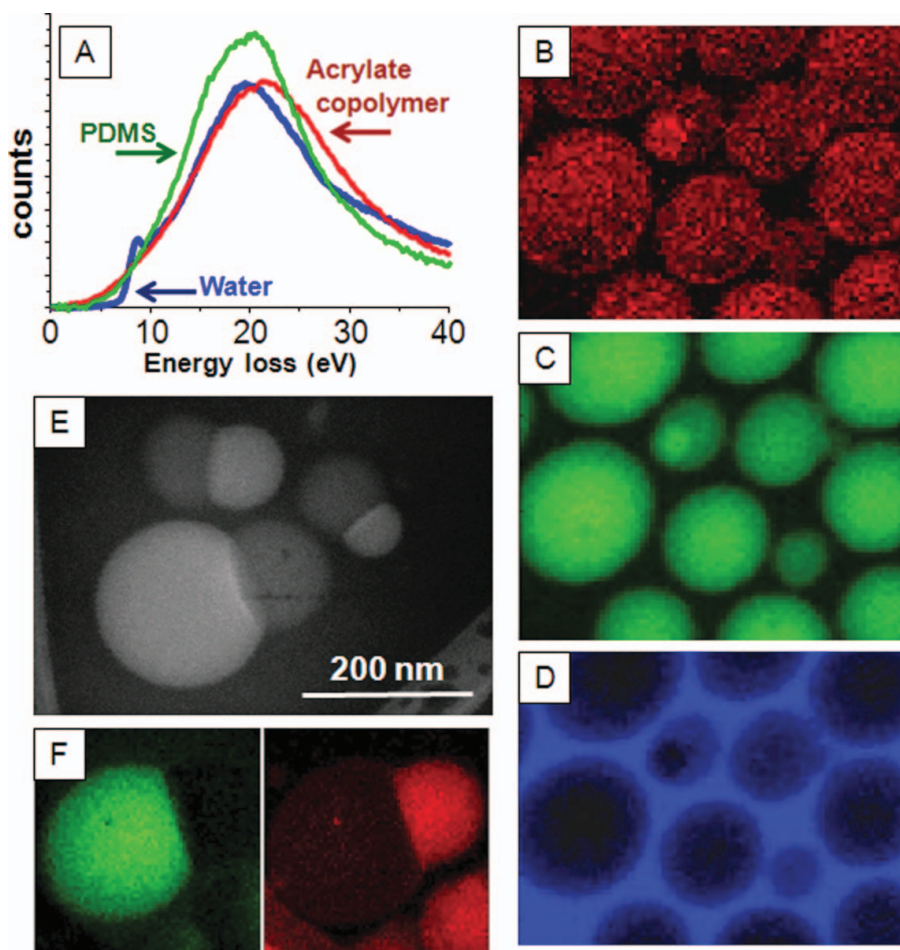


Figure 4. (A) Low-loss EELS spectra; component maps before polymerization for (B) acrylate monomer, (C) PDMS, and (D) amorphous ice (water); (E) high-angle annular dark-field (HAADF) cryo-STEM image of biphasic particle after polymerization; and (F) component maps for polyacrylate (right) and PDMS (left) after polymerization (after Kim et al.⁷⁴). (Figure available in color online)

These studies do, however, suggest that monochromatic energy sources will be able to reveal substantial fine structure in both low-loss and core-loss EELS spectra. In addition, the past two decades have seen substantial work using ultraviolet photoelectron spectroscopy (UPS),^{90–94} which can probe the valence electron structure up to binding energies of about 40 eV, again with energy resolution on the order of 0.05–0.35 eV. These studies also resolve a rich electronic structure in a variety of different polymeric materials. Such spectral information can not only provide new and better fingerprints to give sharper contrast in spectroscopic imaging studies but new insights to electronic structure, particularly at interfaces in a range of emerging soft electronic devices. Electron monochromators are being increasingly used in studies of inorganic materials but have not yet seen much application to polymeric materials. Instrumentation that can provide <30-meV energy resolution with sub-nanometer spatial resolution is planned for commercial production.⁸⁴

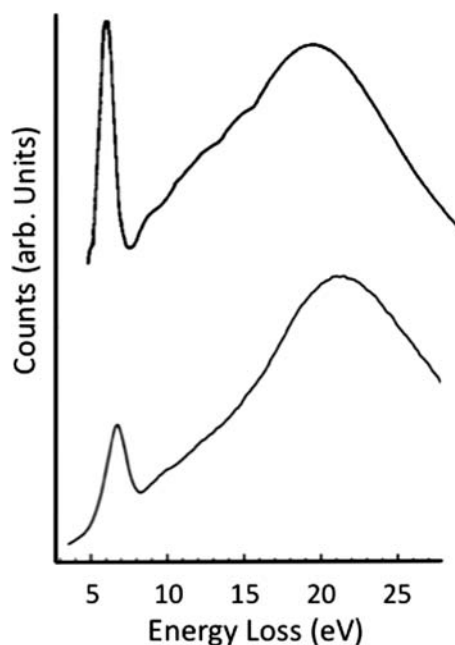


Figure 5. Electron energy-loss spectra from polystyrene. Top: Collected using broad-beam 80-keV incident electrons with 0.11-eV energy resolution (after Ritsko and Bigelow⁸⁶). Bottom: Collected using a focused beam of 200-keV incident electrons with 0.8-eV energy resolution (see Yakovlev and Libera¹¹³).

3. Radiation Damage

Soft materials are well known to undergo structural and chemical change when irradiated with energetic electrons. Collectively, these effects are known as *radiation damage*. Damage is not unique to polymers and biological tissue but is prominent in these soft materials. Metals and semiconductors, by contrast, are relatively insensitive to intermediate-energy electron irradiation. Ceramics, broadly speaking, lie somewhere in between.

The fact that electron microscopes have been used for several decades to characterize soft materials with great success is an important indicator that this tool is one that can answer important morphological questions despite the concerns over radiation damage. Indeed, radiation damage is rarely an issue in studies of stained specimens, because stains tend to stabilize the structure and distribute the deposited energy over larger volumes of material. Furthermore, in studies of unstained specimens at low resolution the incident electron dose can be distributed over relatively large volumes so that the fraction of chemically or structurally modified material remains relatively small. In addition, materials with intrinsic periodicity—e.g., crystalline polymers—lend themselves to signal averaging so the noisy data collected at low incident doses can be combined to create images with high resolution. Variations of this approach have been responsible for many of the successes in macromolecular electron crystallography enjoyed by the biological community.^{95–100} The most challenging soft-materials imaging problems are those on unstained amorphous or aperiodic materials such that data are collected at the highest possible spatial resolution. This is the most general type of problem and is one of increasing importance technologically. At this limit, careful experimentation requires that the effects of radiation damage

be monitored to ensure that the morphological effects being studied are intrinsic to the material and not a consequence of the damage imposed by the experiment itself.

There are two general types of electron–specimen interactions that contribute to damage. One type involves high-angle elastic scattering by atomic nuclei, which can transfer sufficient energy to the specimen to cause atomic displacement. Known as *knock-on* or *displacement* damage, it occurs when the incident energy is above some threshold value that depends on the atomic number and binding energy of the atoms in the specimen. Low-density materials are particularly susceptible to knock-on damage, because of their relatively low atomic mass. The mean displacement energy of carbon in molecular form is approximately 5 eV, and this much energy can be transferred in a head-on (180-degree) collision by incident electrons of energy 30 keV or more.¹⁰¹ In comparison, the threshold energy to displace an atom in crystalline silicon is 145 keV.

A second important type of electron–specimen interaction involves inelastic scattering of incident electrons by atomic electrons. Significantly, the cross sections for both elastic and inelastic electron scattering increase with decreasing incident electron energy. Thus, despite the fact that the effects of knock-on damage due to elastic scattering decreases with decreasing electron energy, the damage due to inelastic scattering increases. Some of the transferred energy is dissipated as heat and under certain circumstances, such as high dose rate and broad-beam illumination of a low-conductivity material, can give rise to an appreciable temperature rise. Calculations suggest, however, that in many practical cases, particularly those involving STEM imaging with a focused electron probe, the temperature rise is limited to a few Kelvin. Often the most significant consequence is mechanical instability of the specimen due to the thermal stresses associated with nonuniform temperature. In the case of low- T_g polymers, however, one must also be aware of beam-induced changes in viscosity and possible local flow.

A more profound consequence of inelastic scattering is that it leads to chemical change in the specimen. The same interactions that are exploited by electron energy-loss spectroscopy to assess chemistry and composition, for example, lead to ionization and bond breaking. The underlying reason is related to the fact that, because most polymers are electrical insulators, there is no ready source of free electrons to saturate a radiation-induced free radical in a timescale shorter than that required for other chemical processes to occur. Among these alternative processes are polymeric chain scission, i.e. depolymerization, or crosslinking, or atomic/molecular motion leading to mass loss. Often these effects can happen simultaneously in a given specimen, because (1) different chemical moieties respond to energetic radiation differently, as manifested by the G -value characterization of radiation sensitivity,¹⁰² (2) the local structural environment can influence whether and how atoms or molecular fragments move, and (3) the local chemical environment can affect the nature of the possible chemical processes that might occur after ionization. Soft materials having high concentrations of aromatic moieties tend to be somewhat more radiation resistant than fully saturated polymers. This property is usually attributed to the delocalization associated with highly conjugated bonds that provide a source of electron charge and the means to distribute the adsorbed energy over a larger volume of material. However, the situation is very different than that, say, for a good metal where there is a vast sea of valence electrons that can fill electron states created by an ionization event and do so on a timescale faster than many of the possible secondary processes that might otherwise occur. Nevertheless, it has been suggested that damage to highly aromatic compounds may require K-ionization of a carbon atom, a relatively dramatic event that leads to Auger emission and a loss of two electrons from the same atom. If so, one might expect damage to cease below some threshold incident energy related to the carbon K-ionization energy

(285 eV) and there is some evidence for this,^{103,104} although the interpretation has been questioned.¹⁰⁵

Practically speaking, radiation damage in soft materials manifests itself in ways that can usually be measured as a function of the incident dose. Chemical changes can be monitored spectroscopically. Changes in crystallinity can be monitored by the fading of intensity in particular Bragg reflections. Mass loss can be monitored by changes in transmission, following a Beers law-type approach. Which of these mechanisms of damage is most important depends on the nature of the morphological questions being asked.

Chemical changes and loss of crystallinity tend to both follow an exponential decay in signal as a function of dose:

$$I(D) = I \exp \left[-\frac{D}{D_c} \right] \quad (3)$$

where D_c is the so-called critical dose (or fluence) at which the signal intensity has fallen to $1/e$ of that characteristic of the unirradiated material. Measuring and reporting D_c for a given experiment is an important part of a careful soft-materials imaging experiment, because it provides a reference for determining the extent to which the doses used during spectral or image data collection cause damage.

Among the unresolved physics associated with radiation damage in soft materials are the delocalized effects that occur tens of nanometers or more from the point of electron incidence. This phenomenon increases the measured critical dose and might, for a point analysis, improve the achievable spatial resolution. First reported by Varlot et al.¹⁰⁶ in 1999 in poly(ethylene terephthalate), it was confirmed by Siangchaew and Libera in polystyrene.¹⁰⁷ In both cases, the dose-dependent decay in the $\pi-\pi^*$ peak associated with aromatic rings was measured by electron energy-loss spectroscopy. When the probe size was decreased from a diameter on the order of $1 \mu\text{m}$ to a diameter on the order of a few nanometers, the apparent critical dose increased by several orders of magnitude. Fast secondary electrons generated by inelastic electron specimen interactions can travel within the plane of the thin specimen, radially away from the incident beam, carrying energy that causes delocalized damage,¹⁰⁷ but their range and number appear to be insufficient to account for the observed increase in D_c . These measurements were based on the 6-7 eV energy-loss peak associated with the $\pi-\pi^*$ excitation and use of the Rayleigh-type formula, $L \sim 0.6\lambda/\langle\theta\rangle$, where $\langle\theta\rangle \sim (0.5E/E_0)^{3/4}$ is a median scattering angle,⁷⁷ gives a delocalization distance $L \sim 4 \text{ nm}$ for $E_0 = 200 \text{ keV}$. An additional contribution to the large D_c values may thus arise from detection of material outside the incident beam that had not yet been damaged by secondary electrons, but this detection involves energy transfer and presumably some damage.

4. Resolution Limits

The limit of spatial resolution in the imaging of polymer morphology using energetic radiation sources is one of increasing interest and importance. This resolution limit is very different from that associated with the imaging of less radiation-sensitive materials such as semiconductors, metals, and many ceramics. In the latter case, the achievable resolution is determined by the quality of the microscope optics, most notably by the spherical aberration of the objective lens, and substantial improvements in resolution have recently been achieved by the development of next-generation aberration correctors¹⁰⁸⁻¹¹¹ and by holography. The so-called point resolution is a well-defined quantity that can be measured and used to reproducibly specify the achievable spatial resolution associated with a particular

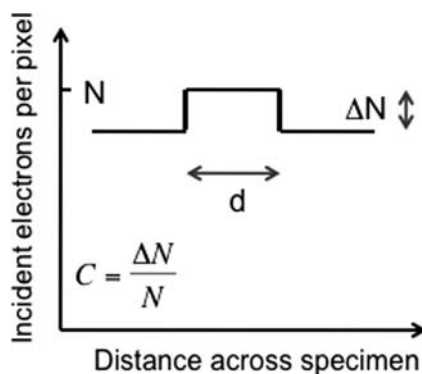


Figure 6. The Rose criterion defines the minimum feature size, d , which contains $N = \Delta N$ counts of intensity, that can be distinguished from the surrounding background with an intensity level of N counts.

microscope and its operating conditions. Achieving this resolution, however, requires relatively high doses of incident radiation. Most inorganic materials can withstand these doses, but most polymers cannot. Consequently, the traditional specification of a microscope's point resolution, or in STEM mode its probe size, is not very useful. Instead one needs to ask what is the minimum dose to which a particular material can be exposed and generate a sufficient signal-to-noise ratio (SNR) so adjacent pixels can be distinguished. This is a well-known problem, first addressed in the 1940s by Albert Rose in the context of television technology^{112,113} and extensively discussed in the context of electron microscopy.^{101,103–105} Some of the insights and limitations of this approach have been discussed by Burgess.¹¹⁴

Rose found that a pattern can be distinguished from a noisy background if the SNR is greater than about 5. We will apply this concept to a single pixel whose lateral dimension is d and whose image intensity, as specified by the number of incident electrons, is N . This intensity differs by an amount ΔN from the background level in adjacent pixels. The contrast ratio is then $C = \Delta N/N$ (Figure 6). If we assume that the noise involved is electron-beam shot noise, which is equal to $N^{1/2}$, then the $\text{SNR} = \Delta N/N^{1/2} = C N^{1/2}$. In order to maximize SNR, we need to increase N until radiation damage threatens to destroy the structure of the specimen, giving $N \sim d^2 D_c/e$ where D_c is the critical dose, and e is the electron charge. Then the Rose criterion becomes $Cd(D_c/e)^{1/2} = \text{SNR} > 5$ so that the smallest useful pixel size (the radiation-limited spatial resolution) is $d = (5/C)(e/D_c)^{1/2}$. For 20% contrast ($C = 0.2$) and $D_c = 0.01 \text{ C/cm}^2$ (typical of many polymers), $d \sim (25) * (D_c/e)^{-1/2} = 1 \text{ nm}$.

For a direct-exposure detector that is capable of counting single electrons,¹¹⁵ this estimate may be realistic. However, most current detectors use a scintillator to convert the electrons into photons, introducing an additional shot-noise term, and the photon detector is a CCD array whose output contains readout noise. Leakage current in the diodes is removed by subtracting the output recorded in the absence of electrons, and this dark-current subtraction increases signal contrast but increases the noise content. Individual CCD diodes have slightly different gain, so the resulting fixed-pattern noise is minimized through division by a flat-field response, but this process again increases the statistical noise. Sousa et al.⁷² measured the standard deviation in the intensity recorded by a CCD detector on a Gatan (Pleasanton, CA) Enfina EELS spectrometer and found it equal to $2.6(N)^{0.48}$, which would increase the smallest useful pixel size to about 2 nm under the above conditions.

In general, the noise performance of an electron detector is described in terms of a detective quantum efficiency (DQE). The actual signal/noise ratio is given by $\text{SNR} = (\text{DQE})^{\frac{1}{2}} (\text{SNR})_{\text{ideal}}$, where $(\text{SNR})_{\text{ideal}}$ is the ideal signal/noise ratio determined by electron-beam shot noise. A more general expression for the damage-limited spatial resolution is therefore:

$$d = (5/C)(e/D_c)^{1/2}(\text{DQE})^{-1/2} \quad (4)$$

This equation presents a useful means with which to estimate the achievable dose-limited resolution. One caveat is that an exposure to a dose as large as D_c involves substantial damage to the specimen, suggesting that the value of d given by Eq. (4) should be regarded as a lower limit. On the other hand, taking $\text{SNR} = 5$ is probably conservative of the signal-to-noise ratio needed to differentiate adjacent pixels.

5. Conclusion and Outlook

The study of polymeric materials using the transmission electron microscope combines challenges and rewards, both in terms of the morphological problems that can be solved as well as the nature of how method and instrument development must occur to better study this class of material. In addition to the well-established and important approach of using heavy element stains to induce contrast between different morphological features, substantial advances have been made over the past two decades in new stain-free imaging methods based either on phase contrast or on spectroscopic contrast. This work is ongoing and will have even greater impact as these new methods become more user friendly and attract the attention of applications-oriented researchers. The damaging effects of the incident ionizing radiation are an ever-present concern, particularly in unstained materials. These effects should not be thought of as a barrier to meaningful morphological measurements in the TEM but rather as an important constraint on how to perform an imaging experiment and how to meaningfully interpret the data.

Acknowledgements

The authors thank Aaron Kuo and Dr. Alex Chou of Stevens for their help with Figure 2 and Dr. Ginam Kim of Dow Corning for his help with Figure 4. M. Libera gratefully acknowledges support from the United States Army Research Office under grant number W911NF-07-1-0543. Ray Egerton acknowledges funding from the Natural Sciences and Engineering Research Council of Canada.

References

1. Williams, D. B.; Carter, C. B. *Transmission electron microscopy: A textbook for materials science*; Plenum: New York, 1996.
2. Egerton, R. F. *Physical principles of electron microscopy: An introduction to TEM, SEM, and AEM*; Springer: New York, 2005.
3. Reimer, L.; Kohl, H. *Transmission electron microscopy: Physics of image formation*, 5th ed.; Springer: New York, 2008.
4. Michler, G. H. *Electron microscopy of polymers*; Springer: Berlin, 2008.
5. Saywer, L. C., Grubb, D. T.; Meyers, G. F. *Polymer microscopy*, 3rd ed.; Springer: New York, 2008.

6. Martin, D. C.; Thomas, E. L. "Experimental high-resolution electron microscopy of polymers," *Polymer*, **1995**, *36*, 1743–1759.
7. Martin, D. C.; Chen, J.; Yang, J.; Drummy, L. F.; Kubel, C. "High resolution electron microscopy of ordered polymers and organic molecular crystals: Recent developments and future possibilities," *Journal of Polymer Science, Part B: Polymer Physics*, **2005**, *43*, 1749–1778.
8. Smith, R. W.; Bryg, V. "Staining polymers for microscopical examination," *Rubber Chemistry and Technology*, **2006**, *79*, 520–540.
9. Haubruge, H. G.; Jonas, A. M.; Legras, R. "Staining of poly(ethylene terephthalate) by ruthenium tetroxide," *Polymer*, **2003**, *44*, 3229–3234.
10. Midgely, P. A.; Weyland, M. "3D electron microscopy in the physical sciences: The development of Z-contrast and EFTEM tomography," *Ultramicroscopy*, **2003**, *96*, 413–431.
11. Spontak, R. J.; Williams, M. C.; Agard, D. A. "Three-dimensional study of cylindrical morphology in a styrene-butadiene-styrene block copolymer," *Polymer*, **1988**, *29*, 387–395.
12. Spontak, R. J.; Smith, S. D.; Agard, D. A. "Electron tomography of microstructural elements in strongly segregated block copolymers," *Proceedings—Annual Meeting, Microscopy Society of America*, **1993**, 888–889.
13. Jinnai, H.; Spontak, R. J. "Transmission electron microtomography in polymer research," *Polymer*, **2009**, *50*, 1067–1087.
14. Chou, T. M.; Prayoonthong, P.; Aitouchen, A.; Libera, M. "Nanoscale artifacts in RuO₄-stained poly(styrene)," *Polymer*, **2002**, *43*, 2085–2088.
15. Wang, Y.; Coombs, N.; Turak, A.; Lu, Z. H.; Manners, I.; Winnik, M. A. "Interfacial staining of a phase-separated block copolymer with ruthenium tetroxide," *Macromolecules*, **2007**, *40*, 1594–1597.
16. Gajdardziska-Josifovska, M.; Carim, A. "Applications of Electron Holography," in *Introduction to electron holography*; Volkl, E., Allard, L., and Joy, D., Eds.; Plenum, New York, 1999; pp. 241–268.
17. Wang, Y. C.; Chou, T. M.; Libera, M.; Voelkl, E.; Frost, B. G. "Measurement of polystyrene mean inner potential by transmission electron holography of latex spheres," *Microscopy and Microanalysis*, **1998**, *4*, 146–157.
18. Wanner, M.; Bach, D.; Gerthson, D.; Werner, R.; Tesche, B. "Electron holography of thin amorphous carbon films: Measurement of the mean inner potential and a thickness-independent phase shift," *Ultramicroscopy*, **2006**, *106*, 341–345.
19. Lunt, R. R.; Kena-Cohen, S.; Benziger, J. B.; Forrest, S. R. "Measurement of the mean inner potentials of anthracene and naphthalene," *Physical Review Letters*, **2009**, *102*, 065504–065507.
20. Petermann, J.; Gleiter, H. "Direct observation of amorphous and crystalline regions in polymers by defocus imaging," *Philosophical Magazine*, **1975**, *31*, 929–934.
21. Liu, T.; Tjiu, W. C.; Petermann, J. "Transmission electron microscopy observations on fine structures of shish-kebab crystals of isotactic polystyrene by partial melting," *Journal of Crystal Growth*, **2002**, *243*, 218–223.
22. Christner, G.; Thomas, E. L. "Visualization of polymer interfaces by phase contrast ("defocus") electron microscopy," *Journal of Applied Physics*, **1977**, *48*, 4063–4067.
23. Roche, E. J.; Thomas, E. L. "Defocus electron microscopy of multiphase polymers: Use and misuse," *Polymer*, **1981**, *22*, 333–341.
24. Handlin, Jr., D. L.; Thomas, E. L. "Phase contrast imaging of styrene-isoprene and styrene-butadiene block copolymers," *Macromolecules*, **1983**, *16*, 1514–1525.
25. Handlin, Jr., D. L.; Thomas, E. L. "Visualization of ordered spherical microdomains of block copolymers by phase contrast electron microscopy," *Journal of Materials Science Letters*, **1984**, *3*, 137–140.
26. Simon, P.; Adhikari, R.; Lichte, H.; Michler, G. H.; Langela, M. "Electron holography and afm studies on styrenic block copolymers and a high impact polystyrene," *Journal of Applied Polymer Science*, **2005**, *96*, 1573–1583.
27. Tonomura, A. *Electron holography*; Springer: Berlin, 1993.
28. Volkl, E.; Allard, L.; Joy, D. *Introduction to electron holography*; Plenum: New York, 1999.

29. Blackson, J. H.; Zhang, X.; Joy, D. C. "Electron Holography of Polymer Blends," in *Proceedings of the 52nd annual meeting of the microscopy society of america*; Bailey, G. W., and Garratt-Reed, A. J., Eds.; San Francisco Press: San Francisco, 1994; 126–127.
30. Libera, M.; Gajdardziska-Josifovska, M.; Disko, M. M. "Off-Axis Electron Holography of a Two-Phase Polymer," in *Proceedings of the 52nd annual meeting of the microscopy society of america*; Bailey, G. W., and Garratt-Reed, A. J., Eds.; San Francisco Press: San Francisco, 1994; 444–445.
31. Libera, M.; Ott, J.; Wang, Y. C. "Transmission Electron Holography of Polymer Microstructure," in *Electron holography*; Tonomura, A.; Allard, L. F.; Pozzi, G.; Joy, D. C.; Ono, Y. A. Eds.; Elsevier: Amsterdam, 1995; pp. 231–237.
32. Simon, P.; Huhle, R.; Lehmann, M.; Lichte, H.; Monter, D.; Bieber, T.; Reschetilowski, W.; Adhikari, R.; Michler, G. H. "Electron holography on beam sensitive materials: Organic polymers and mesoporous silica," *Chemistry of Materials*, **2002**, *14*, 1505–1514.
33. Chou, T. M.; Libera, M.; Gauthier, M. "Quantitative phase contrast imaging of arborescent graft polystyrene by off-axis transmission electron holography," *Polymer*, **2003**, *44*, 3037–3043.
34. Simon, P.; Lichte, H.; Drechsel, J.; Formanek, P.; Graff, A.; Wahl, R.; Mertig, M.; Adhikari, R.; Michler, G. H. "Electron holography of organic and biological materials," *Advanced Materials*, **2003**, *15*, 1475–1481.
35. Simon, P.; Maennig, B.; Lichte, H. "Conventional electron microscopy and electron holography of organic solar cells," *Advanced Functional Materials*, **2004**, *14*, 669–676.
36. Simon, P.; Lichte, H.; Formanek, P.; Lehmann, M.; Huhle, R.; Carrillo-Cabrera, W.; Harscher, A.; Ehrlich, H. "Electron holography of biological samples," *Micron*, **2008**, *39*, 229–256.
37. Danev, R.; Glaeser, R. M.; Nagayama, K. "Practical factors affecting the performance of a thin-film phase plate for transmission electron microscopy," *Ultramicroscopy*, **2009**, *109*, 312–325.
38. Mtasumoto, T.; Tonomura, A. "The phase constancy of electron waves traveling through boersch's electrostatic wave plate," *Ultramicroscopy*, **1997**, *63*, 5–10.
39. Majorovits, E.; Barton, B.; Schultheriss, K.; Perez-Willard, F.; Gerthsen, B.; Schroder, R. R. "Optimizing phase contrast in transmission electron microscopy with an electrostatic (boersch) phase plate," *Ultramicroscopy*, **2007**, *107*, 213–226.
40. Malac, M.; Belaggia, M.; Egerton, R. F.; Zhu, Y. "Imaging of radiation-sensitive samples in transmission electron microscopes equipped with zernike phase plates," *Ultramicroscopy*, **2008**, *108*, 126–140.
41. Tosaka, M.; Danev, R.; Nagayama, K. "Application of phase contrast transmission microscopic methods to polymer materials," *Macromolecules*, **2005**, *38*, 7884–7886.
42. Egerton, R. F. *Electron energy loss spectroscopy in the electron microscope*, 2nd ed.; Plenum: New York, 1996.
43. Egerton, R. F. "Electron energy-loss spectroscopy in the TEM," *Reports on Progress in Physics*, **2009**, *72*, 016502.
44. Ahn, C. C., Ed. *Transmission electron energy loss spectrometry in materials science and the EELS atlas*, 2nd ed.; Wiley-VCH: Weinheim, 2004.
45. Jeanguillaume, C.; Colliex, C. "Spectrum-imaging: the next step in EELS digital acquisition and processing," *Ultramicroscopy*, **1988**, *28*, 252–257.
46. Hunt, J. A.; Williams, D. B. "Electron energy-loss spectrum-imaging," *Ultramicroscopy*, **1991**, *38*, 47–73.
47. Hofer, F.; Warbichler, P. "Elemental Mapping Using Energy Filtered Imaging," in *Transmission electron energy loss spectrometry in materials science and the EELS atlas*, Ahn, C., Ed.; Wiley-VCH: Wienheim, 2004; pp. 159–222.
48. Linares, E. M.; Leite, C. A. P.; Valadares, L. F.; Silva, C. A.; Rezende, C. A.; Galembeck, F. "Molecular mapping by low-energy-loss energy-filtered transmission electron microscopy," *Analytical Chemistry*, **2009**, *81*, 2317–2324.
49. Du Chesne, A. "Energy filtering transmission electron microscopy of polymers—benefit and limitations of the method," *Macromolecular Chemistry and Physics*, **1999**, *200*, 1813–1830.

50. Libera, M.; Disko, M. M. "Electron Energy Loss Spectroscopy of Polymers," in *Transmission Electron energy loss spectrometry in materials science*; Ahn, C., Ed.; Wiley-VCH: New York, 2004; 419–454.
51. Ribbe, A. E.; Hayashi, M.; Weber, M.; Hashimoto, T. "Morphology determination of novel polysulfone-polyamide block copolymers using element spectroscopic imaging in the transmission electron microscopy," *Macromolecules*, **2000**, *33*, 2786–2789.
52. Varlot, K.; Martin, J. M.; Quet, C. "Phase differentiation of a tri-phase polymer composite using energy-filtering transmission electron microscopy," *Polymer*, **2000**, *41*, 4599–4605.
53. Rippel, M. M.; Leite, C. A. P.; Galembek, F. "Elemental mapping in natural rubber latex films by electron energy loss spectroscopy associated with transmission electron microscopy," *Analytical Chemistry*, **2002**, *74*, 2541–2546.
54. Yamauchi, K.; Takahashi, K.; Hasegawa, H.; Iatrou, H.; Hadjichristidis, N.; Kaneko, T.; Nishikawa, Y.; Jinnai, H.; Matsui, T.; Nishioka, H.; Shimizu, M.; Furukawa, H. "Microdomain morphology in an ABC 3-miktoarm star terpolymer: A study by energy-filtering TEM and 3D electron tomography," *Macromolecules*, **2003**, *36*, 6962–6966.
55. Correa, C. A.; Bonse, B. C.; Chinaglia, C. R.; Hage, Jr., E.; Pessan, L. A. "Characterization of unstained multiphase polymer systems by analytical electron microscopy," *Polymer Testing*, **2004**, *23*, 775–778.
56. Rippel, M. M.; Leite, C. A. P.; Lee, L. T.; Galembek, F. "Direct imaging and elemental mapping of microgels in natural rubber particles," *Colloid and Polymer Science*, **2005**, *283*, 570–574.
57. Hayakawa, T.; Goseki, R.; Kakimoto, M. A.; Tokita, M.; Watanabe, J.; Liao, Y.; Horiuchi, S. "Self-assembled lamellar nanostructures of wholly aromatic rod-rod-type block molecules," *Organic Letters*, **2006**, *8*, 5453–5456.
58. Sousa, A.; Sengonul, M.; Latour, R.; Kohn, J.; Libera, M. "Selective protein adsorption on a phase-separated solvent-cast polymer blend," *Langmuir*, **2006**, *22*, 6286–6292.
59. Gomez, E. D.; Panday, A.; Feng, E. H.; Chen, V.; Stone, G. M.; Minor, A. M.; Kisielowski, C.; Downing, K. H.; Borodin, O.; Smith, G. D.; Balsara, N. P. "Effect of ion distribution on conductivity of block copolymer electrolytes," *Nano Letters*, **2009**, *9*, 1212–1216.
60. Horiuchi, S.; Hanada, T.; Ebisawa, M.; Matsuda, Y.; Kobayashi, M.; Takahara, A. "Contamination-free transmission electron microscopy for high-resolution carbon elemental mapping of polymers," *ACS Nano*, **2009**, *3*, 1297–1304.
61. Arayasantiparb, D.; McKnight, S.; Libera, M. "Compositional variation within the epoxy/adherend interphase," *Journal of Adhesion Science and Technology*, **2001**, *15*, 1463–1484.
62. Horiuchi, S.; Hamanaka, T.; Aoki, T.; Miyakawa, T.; Narita, R.; Wakabayashi, H. "Characterization of polymer-adhesive interfaces on a nanometre scale by elemental mapping and image EELS using EFTEM," *Journal of Electron Microscopy*, **2003**, *52*, 255–266.
63. Horiuchi, S.; Yin, D.; Ougizawa, T. "Nanoscale analysis of polymer interfaces by energy-filtering transmission electron microscopy," *Macromolecular Chemistry and Physics*, **2005**, *206*, 725–731.
64. Horiuchi, S.; Dohi, H. "Nanoimaging and spectroscopic analysis of rubber/zno interfaces by energy-filtering transmission electron microscopy," *Langmuir*, **2006**, *22*, 4607–4613.
65. Horiuchi, S.; Yin, D.; Liao, Y.; Ougizawa, T. "Study of adhesion and fracture of polymer laminates by imaging of interfaces," *Macromolecular Rapid Communications*, **2007**, *28*, 915–921.
66. Liao, Y.; Nakagawa, A.; Horiuchi, S.; Ougizawa, T. "Interdiffusion at homopolymer/random copolymer interfaces investigated by energy-filtering transmission electron microscopy," *Macromolecules*, **2007**, *40*, 7966–7972.
67. Gomez, E. D.; Ruegg, M. L.; Minor, A. M.; Kisielowski, C.; Downing, K. H.; Glaeser, R. M.; Balsara, N. P. "Interfacial concentration profiles of rubbery polyolefin lamellae determined by quantitative electron microscopy," *Macromolecules*, **2008**, *41*, 156–162.
68. Bertho, J.; Stolojan, V.; Abel, M. L.; Watts, J. F. "The effect of silane incorporation on a metal adhesive interface: A study by electron energy loss spectroscopy," *Micron*, **2010**, *41*, 130–134.

69. Sun, S.; Shi, S.; Leapman, R. D. "Water distributions of hydrated biological specimens by valence electron energy loss spectroscopy," *Ultramicroscopy*, **1993**, *50*, 127–139.
70. Sun, S. Q.; Shi, S.-L.; Hunt, J. A.; Leapman, R. D. "Quantitative water mapping of cryosectioned cells by electron energy-loss spectroscopy," *Journal of Microscopy*, **1995**, *177*, 18–30.
71. Kim, G.; Sousa, A.; Meyers, D.; Shope, M.; Libera, M. "Diffuse polymer interfaces in lobed nanoemulsions preserved in aqueous media," *Journal of the American Chemical Society*, **2006**, *128*, 6570–6571.
72. Sousa, A.; Aitouchen, A.; Libera, M. "Water mapping in hydrated soft materials," *Ultramicroscopy*, **2006**, *106*, 130–145.
73. Sousa, A.; Schut, J.; Kohn, J.; Libera, M. "Nanoscale morphological changes during hydrolytic degradation and erosion of a bioresorbable polymer," *Macromolecules*, **2006**, *39*, 7306–7312.
74. Kim, G.; Sousa, A.; Meyers, D.; Libera, M. "Nanoscale composition of biphasic polymer nanocolloids in aqueous suspension," *Microscopy and Microanalysis*, **2008**, *14*, 459–468.
75. Yakovlev, S.; Libera, M. "Cryo-stem eels of nafion saturated with an organic solvent," *Microscopy and Microanalysis*, **2006**, *12*, 996–997.
76. Yakovlev, S.; Misra, M.; Shi, S.; Libera, M. "Specimen thickness dependence of hydrogen evolution during cryo-transmission electron microscopy of hydrated soft materials," *Journal of Microscopy*, **2009**, *236*, 174–179.
77. Parravicini, G. P.; Resca, L. "Electronic states and optical properties in cubic ice," *Physical Review B*, **1973**, *8*, 3009–3023.
78. Egerton, R. F. "New techniques in electron energy-loss spectroscopy and energy-filtered imaging," *Micron*, **2003**, *34*, 127–139.
79. Kothleitner, G.; Hofer, F. "EELS performance measurements on a new high energy resolution imaging filter," *Micron*, **2003**, *34*, 211–218.
80. Kimoto, K.; Kothleitner, G.; Grogger, W.; Matsui, Y.; Hofer, F. "Advantages of a monochromator for bandgap measurements using electron energy-loss spectroscopy," *Micron*, **2005**, *36*, 185–189.
81. Lazar, S.; Botton, G. A.; Zandbergen, H. W. "Enhancement of resolution in core-loss and low-loss spectroscopy in a monochromated microscope," *Ultramicroscopy*, **2006**, *106*, 1091–1103.
82. Egerton, R. F. "Limits to the spatial, energy and momentum resolution of electron energy-loss spectroscopy," *Ultramicroscopy*, **2007**, *107*, 575–586.
83. Dahmen, U.; Erni, R.; Radmilovic, V.; Kisielowski, C.; Rossell, M. D.; Denes, P. "Background, status and future of the transmission electron aberration-corrected microscope project," *Philosophical Transactions of the Royal Society A: Mathematical, Physical and Engineering Sciences*, **2009**, *367*, 3795–3808.
84. Krivanek, O. L.; Ursin, J. P.; Bacon, N. J.; Corbin, G. J.; Dellby, N.; Hrnčirik, P.; Murfitt, M. F.; Own, C. S.; Szilagy, Z. S. "High-energy-resolution monochromator for aberration-corrected scanning transmission electron microscopy/electron energy-loss spectroscopy," *Philosophical Transactions of the Royal Society A*, **2009**, *367*, 3683–3697.
85. Katterwe, H. "Object Analysis by Electron Energy Loss Spectroscopy in the Infra-Red Region," in *Electron microscopy—1972*; Cosslet, V. E., Ed.; The Institute of Physics: London, 1972; pp. 154–155.
86. Ritsko, J. J.; Bigelow, R. W. "Core excitons and the dielectric response of polystyrene and poly(2-vinylpyridine) from 1 to 400 ev," *Journal of Chemical Physics*, **1978**, *69*, 4162–4170.
87. Ritsko, J. J. "Electron energy loss spectroscopy of pristine and radiation damaged polyethylene," *Journal of Chemical Physics*, **1979**, *70*, 5343–5349.
88. Fink, J.; Scheerer, B.; Stamm, M.; Tieke, B.; Kanellakopoulos, B.; Dornberger, E. "Electronic structure of li-doped polyparaphenylene," *Physical Review B*, **1984**, *30*, 4867–4869.
89. Fink, J.; Scheerer, B.; Wernet, W.; Monkenbusch, M.; Wegner, G.; Freund, H.-J.; Gonska, H. "Electronic structure of pyrrole-based conducting polymers: An electron-energy-loss-spectroscopy study," *Physical Review B*, **1986**, *34*, 1101–1115.
90. Duke, C. B.; Salaneck, W. R.; T.J., F.; Ritsko, J. J.; Thomas, H. R.; Paton, A. "Electronic structure of pendant-group polymers: molecular-ion states and dielectric properties of poly(2-vinyl pyridine)," *Physical Review B*, **1978**, *18*, 5717–5739.

91. Beamson, G. "Conformation effects in the xps valence band spectra of aliphatic polyesters," *Journal of Electron Spectroscopy and Related Phenomena*, **2007**, *154*, 83–89.
92. French, R. H.; Winey, K. I.; Yang, M. K.; Qiu, W. "Optical properties and van der waals-london dispersion interactions of polystyrene determined by vacuum ultraviolet spectroscopy and spectroscopic ellipsometry," *Australian Journal of Chemistry*, **2007**, *60*, 251–263.
93. Ueno, N.; Kera, S. "Electron spectroscopy of functional organic thin films: Deep insights into valence electronic structure in relation to charge transport property," *Progress in Surface Science*, **2008**, *83*, 490–557.
94. Salaneck, W. R. "Classical ultraviolet photoelectron spectroscopy of polymers," *Journal of Electron Spectroscopy and Related Phenomena*, **2009**, *174*, 3–9.
95. De Rosier, D. J.; Klug, A. "Reconstruction of three dimensional structures from electron micrographs," *Nature*, **1968**, *217*, 130–134.
96. Frank, J. "Averaging of low exposure electron micrographs of non periodic objects," *Ultramicroscopy*, **1975**, *1*, 159–162.
97. van Heel, M.; Frank, J. "Use of multivariate statistics in analysing the images of biological macromolecules," *Ultramicroscopy*, **1981**, *6*, 187–194.
98. van Heel, M. "Classification of very large electron microscopical image data sets," *Optik*, **1989**, *82*, 114–126.
99. Frank, J. "Single-particle imaging of macromolecules by cryo-electron microscopy," *Annual Review of Biophysics and Biomolecular Structure*, **2002**, *31*, 303–319.
100. Subramaniam, S.; Milne, J. L. S. "Three-dimensional electron microscopy at molecular resolution," *Annual Review of Biophysics and Biomolecular Structure*, **2004**, *33*, 141–155.
101. Reimer, L.; Kohl, H. *Transmission electron microscopy: Physics of image formation*; Springer: Berlin, 2008.
102. Chapiro, A. *Radiation chemistry of polymeric systems*; Plenum: New York, 1962.
103. Howie, A. "Radiation damage problems in electron microscopy," *Revue de Physique Applique*, **1980**, *15*, 291–295.
104. Glaeser, R. "Retrospective: radiation damage and its associated 'information limitations'," *Journal of Structural Biology*, **2008**, *163*, 271–276.
105. Yakovlev, S.; Libera, M. "Dose-limited spectroscopic imaging of soft materials by low-loss EELS in the scanning transmission electron microscope," *Micron*, **2008**, *39*, 734–740.
106. Varlot, K.; Martin, J. M.; Gonbeau, D.; Quet, C. "Chemical bonding analysis of electron-sensitive polymers by EELS," *Polymer*, **1999**, *20*, 5691–5697.
107. Siangchaew, K.; Libera, M. "Influence of fast secondary electrons on the aromatic structure of polystyrene," *Philosophical Magazine*, **2000**, *80*, 1001–1016.
108. Haider, M.; Rose, H.; Uhlemann, S.; Schwan, E.; Kabius, B.; Urban, K. "A spherical-aberration-corrected 200 kv transmission electron microscope," *Ultramicroscopy*, **1998**, *75*, 53–60.
109. Evans, J. E.; Hetherington, C.; Kirkland, A.; Chang, L. Y.; Stahlberg, H.; Browning, N. "Low-dose aberration corrected cryo-electron microscopy of organic specimens," *Ultramicroscopy*, **2008**, *108*, 1636–1644.
110. Smith, D. J. "Development of aberration-corrected electron microscopy," *Microscopy and Microanalysis*, **2008**, *14*, 2–15.
111. Urban, K. W. "Studying atomic structures by aberration-corrected transmission electron microscopy," *Science*, **2008**, *321*, 506–510.
112. Rose, A. "Television Pickup Tubes and the Problem of Vision," in *Advances in electronics*; Marton, L., Ed.; Academic Press: New York, 1948; 131–166.
113. Rose, A. *Vision: Human and electronic*; Plenum: New York, 1973.
114. Burgess, A. E. "The rose model, revisited," *Journal of the Optical Society of America A*, **1999**, *16*, 633–646.
115. McMullan, G.; Chen, S.; Henderson, R.; Faruqi, A. R. "Detective quantum efficiency of electron area detectors in electron microscopy," *Ultramicroscopy*, **2009**, *109*, 1126–1143.